High temperature oxidation and creep behavior of pre-oxidized zircaloy-4 claddings under loca conditions

E-B Djeumen, Nicolas Tardif, Jean Desquines, Tatiana Taurines, Gergely Molnár, M.-C Baietto, Michel Coret, Alice Viretto, G. Villevieille, Philippe Chaudet

HIGH TEMPERATURE OXIDATION AND CREEP BEHAVIOR OF PRE-OXIDIZED ZIRCALOY-4 CLADDINGS UNDER LOCA CONDITIONS

E.-B Djeumen[1,2], N. Tardif[2], J. Desquines[1], T. Taurines[1], G. Molnár[2], M.-C Baietto[2], M. Coret[3], A. Viretto[1], G. Villevieille[1], P. Chaudet[2]

[1]IRSN, PSN-RES/SEREX/LE2M, Cadarache, St Paul-Lez-Durance, France

[2]University of Lyon, INSA-Lyon, CNRS UMR5259, LaMCoS, F-69621, France

[3]University of Nantes, Central School of Nantes, CNRS UMR6183, GeM, France

ABSTRACT

During a LOCA, fuel claddings in a pressurised water reactor can be subjected to severe thermo-mechanical loadings. The temperature of the claddings can reach more than 1000°C and the pressure difference between the inside and the outside of the cladding can exceed 100 bar. During normal operation of the reactor, the claddings are corroded by primary water. In accidental situations, the oxidation of the cladding is strongly influenced by its temperature. This work aims to study the thermo-mechanical behavior of the cladding under such loading conditions, considering its corrosion state. Several coupled physics affect the behavior of the cladding under such conditions. These include the coupling between metal and oxide creep, oxygen diffusion into the metal, oxidation and oxide damage. On one hand, oxidation tests are carried out at 750°C and 820°C in order to study the oxidation of the claddings without external mechanical loadings. At these temperatures, a cubic kinetics is observed for oxide growth. The growth kinetics of the oxygen enriched metal layer (α(O)) is consistent with the extrapolation of the correlation established by other studies, from tests performed at higher temperatures (T>900°C). This result was not obvious because the material undergoes a phase transformation between 820°C and 900°C. The metal oxygen diffusion coefficient identified at 750°C and 820°C are consistent with previous work. On the other hand, semi-integral ballooning tests involving the coupling between mechanical loading and high temperature oxidation are carried out. These tests demonstrate the strengthening role of the pre-oxide, high temperature oxide and α(O) with respect to creep. This reinforcing role is strongly reduced once the oxide layer progressively cracks finally leading ballooning onset.

1. Introduction

The thermomechanical behavior of a pre-oxidized cladding in a LOCA is affected by several coupled physics. This includes couplings between metal and oxide creep, oxygen diffusion, oxidation and oxide damage. A separate effect experimental approach is used to study these couplings. First, High Temperature (HT) oxidation tests are performed to characterize oxygen diffusion in the metal without applied mechanical loading. Second, internal pressure ballooning tests involving oxygen diffusion and creep are performed. The final objective of this work is to highlight the oxygen and corrosion layer effects on the ballooning of the cladding during a LOCA.

2. HT oxidation tests

2.1. Materials

The material of the study is Stress Relieved Annealed (SRA) Zircaloy-4. The as-fabricated material composition is summarized in Tab 1.

Sn (wt%)	Fe (wt%)	Cr(wt%)	O(wt%)	H(wppm)
1.30	0.21	0.11	0.14	15

Tab 1: Zircaloy-4 material composition.

2.2. Test protocols

2.2.1. Study of the oxidation kinetics

The oxidation test protocol is shown in Fig 1. The main steps are:

- Two-sided pre-oxidation of samples at 470°C under air. This step leads to 10µm thick oxide layers on the inner and outer sides.
- Optical metallography measurement of the oxide layer thickness after the pre-oxidation step. Hydrogen content measurements were systematically performed before and after oxidation.
- Argon (with a flow rate of 2nL/min) or a mixture of argon and steam (with respective flow rates of 2nL/min and 100g/h) injection at atmospheric pressure into a vertical furnace preheated to 750°C or 820°C.
- 20mm long samples HT oxidation in the furnace for 400, 800, 1600 or 3200 seconds. HT oxidation ends with water quenching at a cooling rate of approximately -200°C/s [1].
- Optical metallography is used to measure the thickness of the zirconia layer and the oxygen-enriched metal layer α(O) after HT oxidation. These measurements are performed with a Keyence VHX 5000 optical microscope having an accuracy of about 1µm to 2µm. 16 azimuthal measurements were averaged to determine layer thicknesses.
- Finally, a CAMECA-SX100 Castaing microprobe micro-analysis allows determining the oxygen profile with a spatial resolution lower than 1µm. The oxygen profile is determined by averaging 4 azimuthal measurements.

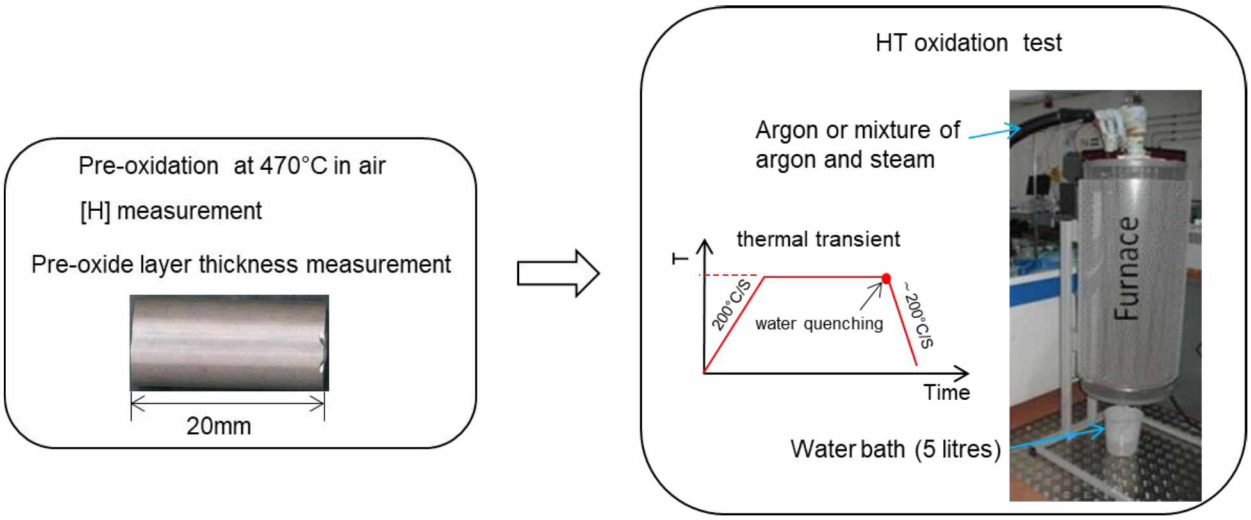

Fig 1: Oxidation test protocol, the samples are pre-oxidized at 470°C under air before being introduced into the furnace at 750°C or 820°C for HT oxidation.

Fig 2 shows the microstructure of a 10µm thick external pre-oxide before HT oxidation. The inner oxide has a comparable microstructure.

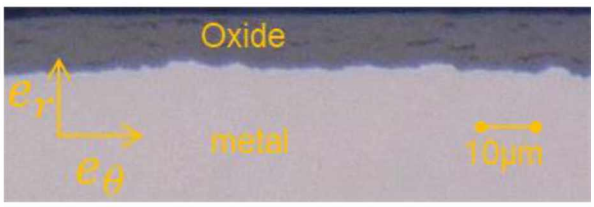

Fig 2: Optical metallography of a 10µm thick pre-oxide.

19 tests were performed, 6 at 750°C and 13 at 820°C. As-fabricated and pre-oxidized samples were tested. The atmosphere test effect was also studied. A test (A8) was carried out on an as-fabricated sample on which a paint layer was deposited. The paint is used for kinematical optical full field measurement during the ballooning tests (see section 2.2.2). This was done in order to study is the potential intrusive effect of the paint on the oxidation.

Sample ID	Outer pre-oxide layer thickness (µm)	Hydrogen content before HT oxidation (wppm)	HT oxidation temperature (°C)	Oxidation duration (s)	HT oxidation conditions
A1	As fabricated No pre-oxidation	11	750	800	Mixture of argon and steam
A2			750	1600	
A3			750	3200	
A4			820	400	
A5			820	800	
A6			820	1600	
A7			820	3200	
A8 (speckle)			820	3200	
POX1	7.2±1.1	67±1.7	750	800	
POX2	7.3±1.0	70±1.2	750	1600	
POX3	8.4±1.4	69±0.8	750	3200	
POX4	8.4±0.9	70±2.6	820	400	
POX5	7.6±1.3	77±2.6	820	800	
POX6	8.6±0.9	63±2.4	820	1600	
POX7	9.0±1.2	66±0.1	820	3200	
POX8	7.6±1.0	62±1.5	820	400	argon
POX9	7.6±1.0	62±0.5	820	800	
POX10	7.9±0.7	63±1.2	820	1600	
POX11	7.1±0.9	63±1.5	820	3200	

Tab 2: High temperature oxidation test matrix. The uncertainty represents the standard deviation based on sixteen measurements for the pre-oxide thickness and three measurements for the hydrogen content.

2.2.2. Study of the ballooning by creep under internal pressure

Samples tested during the ballooning tests are 90mm long as-fabricated or pre-oxidized Zircaloy-4 cladding tubes. The pre-oxidation is performed with the same protocol described in section 2.2.1. A speckle is deposited on the outer surface of the specimen using Ulfalux®1200°C high temperature coatings. It allows performing digital image correlation measurements. An internal pressure is applied and regulated throughout the test using argon or argon (80%) +O_2 (20%) mixture. The test takes place inside an enclosure in which the same gas used for internal pressurization is used to flush the external surface of the sample at a low flow rate (Fig 3). An axial compression force is applied on the sample to generate a pure circumferential stress state. This compression force F is calculated using the internal radius R_i and the internal pressure P_i:

$$F = -P_i \times \pi \times R_i \quad (1)$$

An induction heating system, consisting of an inductor connected to a 30kW ThermoInduzione power generator, is used to heat the sample. The temperature is regulated by two thermocouples (type K, 79µm diameter) welded on the external surface of the sample. A 12MPx CMOS camera equipped with a near infrared filter is used to follow the region between the inductor coils (the Region Of Interest, ROI) during the tests. This camera is used to perform both kinematic full-field measurements by image correlation and thermal field measurements

by Near InfraRed Thermography (NIRT) [2], [3]. The NIRT links the grey level I of each pixel of the image to its temperature T through a radiometric model based on Planck's law:

$$T = \frac{K_1}{ln\left(\frac{K_2}{I} + 1\right)} \quad (2)$$

The two constants, K_1 and K_2 are calibrated from thermocouples measurements.

The thermal loading is first applied using a heating rate of 3°C/s until a temperature of 800°C. The mechanical loading (internal pressure and axial compression force) is then imposed and maintained in order to observe the cladding creep. The test time is set to zero after the stabilization of the mechanical and thermal loadings.

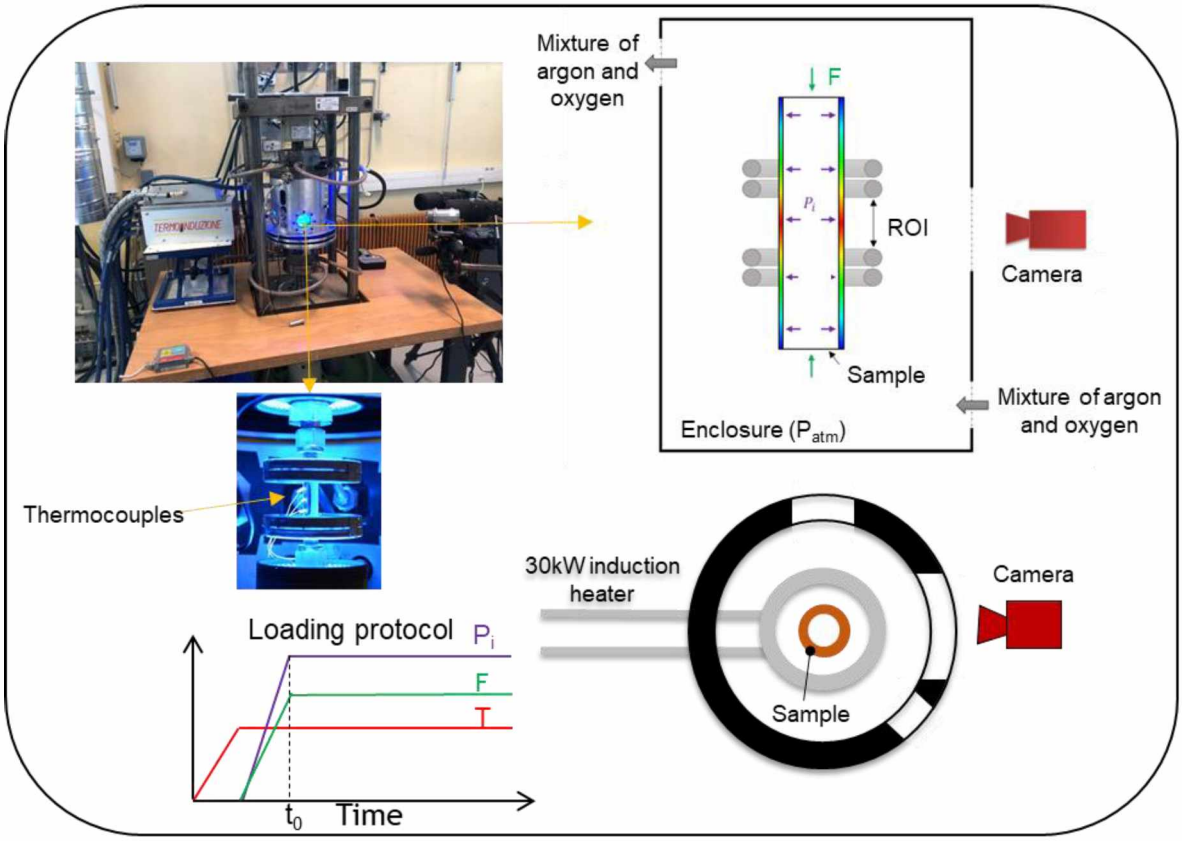

Fig 3: Ballooning test in the ELLIE device.

Tab 3 summarizes performed ballooning tests. Two tests were performed on as-fabricated samples and three on pre-oxidized samples.

Sample ID	Inner /outer oxide layer thickness (µm)	Test duration (s)	T at the middle of the sample during the test (°C) Uncertainty is about 7°C	Test conditions
As-fab1	As fabricated No pre-oxidation	burst	[811-814]	Argon only
As-fab2		1300	[808-818]	Argon + O_2
Ballox1	9.1 ± 0.4	10	[802-808]	
Ballox2	10.5 ± 0.3	100	[805-810]	
Ballox3	10.1 ± 0.6	burst	[799-805]	

Tab 3: Ballooning test matrix, all tests are performed under a 30 bar internal pressure and at a constant temperature of 800°C. The temperature uncertainty is about 7°C [2].

3. Experimental results

3.1. HT oxidation tests

3.1.1. Pre-oxide colour change

Fig 4 shows POX11 sample before and after HT oxidation at 820°C under argon for 3200s.

Fig 4: Pre-oxide colour change after HT oxidation at 820°C under argon for 3200s.

The initially beige oxide becomes black after HT oxidation. This colour change is a subject of discussion, its origin is generally attributed to the diffusion of oxygen from the oxide to the metal leading to a sub-stoichiometric oxide layer. This phenomenon occurs very quickly and has been observed in all tests performed on pre-oxidized samples.

3.1.2. Growth of oxide, α(O) and hydrogen uptake

The hydrogen uptake observed after HT oxidation is very low, less than 60 wppm for all tests. The tests performed on the pre-oxidized samples did not reveal any variation in oxide layer thickness. The pre-oxide has a protective role, limiting HT oxidation, for the investigated temperatures and durations. The formation of HT oxide was observed only on as-fabricated samples. The microstructure of the HT oxide is not porous (Fig 5.a) unlike that of the pre-oxide (Fig 1). The time evolution of the HT oxide layers thickness is plotted in Fig 5.b. According to the literature the oxidation kinetics follows a cubic law [4] for temperatures around 800°C:

$$e_{ZrO_2} = k_T \times t^{1/3} \tag{3}$$

k_T: is a constant that depends on the temperature T.

The values $k_{750°C} = 0.44\ \mu m \cdot s^{-1/3}$, $k_{820°C} = 0.68\ \mu m \cdot s^{-1/3}$ adequately represent the experimental data.

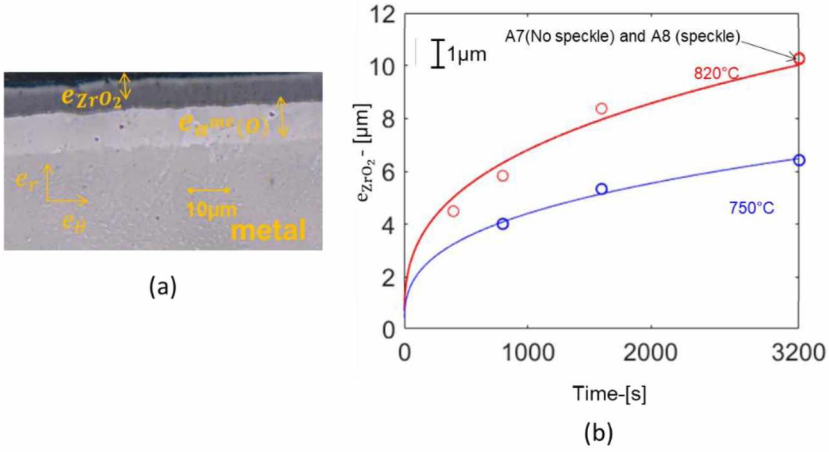

Fig 5: (a) Optical metallography of A7 sample after HT oxidation, (b) HT outer oxide thickness versus oxidation time on as-fabricated samples at 750°C and 820°C.

Fig 5.b shows that the speckle has no influence on the HT oxide growth kinetics.

During HT oxidation, an oxygen enriched layer called α(O) is formed in the metal beneath the oxide due to the diffusion of oxygen from the oxide to the metal. This layer appears lighter than the metal on the optical metallography as shown in Fig 5.a.

Fig 6.a shows the time evolution of the α(O) layer thickness measured by optical metallography. These results are compared with the extrapolation of the IRSN law established from tests performed at higher temperatures (900°C<T<1200°C) [1]:

$$e_{\alpha^{me}(O)}(\mu m) = \sqrt{3.78.10^{7}\, exp\left(-\frac{21557}{T}\right) t(s)} \qquad (4)$$

$e_{\alpha^{me}(O)}$: α(O) thickness measured by optical metallography.

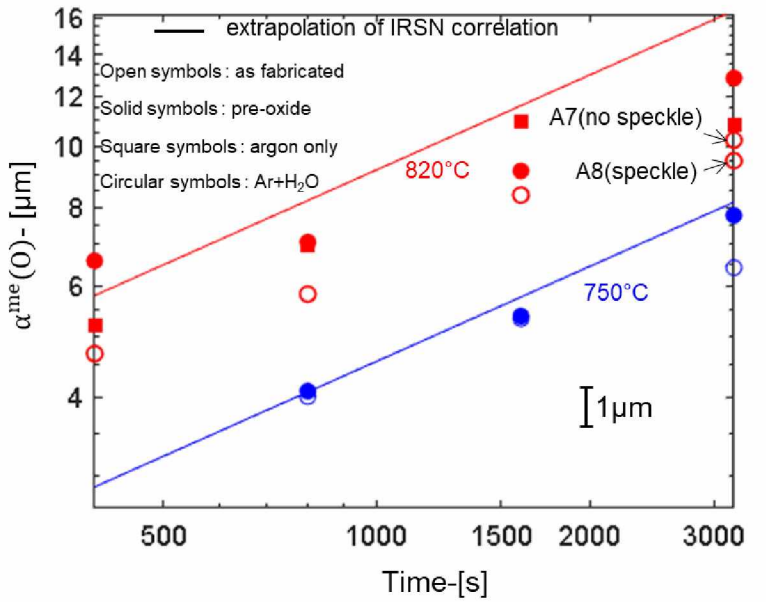

Fig 6: Time evolution of the α(O) layer thickness, the results obtained in this work are compared to the extrapolation of the IRSN correlation.

The results obtained in this work are consistent with the extrapolation of the IRSN law. The influence of the pre-oxide on the α(O) layer thickness formed during HT oxidation seems negligible. The α(O) layer thickness on as-fabricated samples and on pre-oxidized samples are comparable, even if the α(O) layer thickness on the as-fabricated sample tends to be lower than that on pre-oxidized samples at 750°C and 820°C. The environment also seems to have no influence on the α(O) layer of pre-oxidized samples, indeed tests at 820°C under argon and steam mixture lead to the same α(O) layer thickness as the tests under argon alone for the same duration. The pre-oxide is a sufficiently large oxygen source for the metal.
The speckle also has no influence on the α(O) growth kinetics. At the temperatures studied, the oxygen concentration that allows distinguishing this layer α(O) from the metal on an optical metallography is not known. Additional microprobe analyses to determine the oxygen profile were performed. The measurement of the oxygen profiles was only carried out on the tests under argon and steam mixture. These HT oxidation tests were also simulated using the phase-field approach based on the finite element method developed in this work. Details concerning this simulation tool will be available in our next article. A FEMU (Finite Element Model Updating) allow to identify the oxygen diffusion coefficient in the metal. Fig 7 shows the comparison between the simulated oxygen profiles and the experimental profiles.

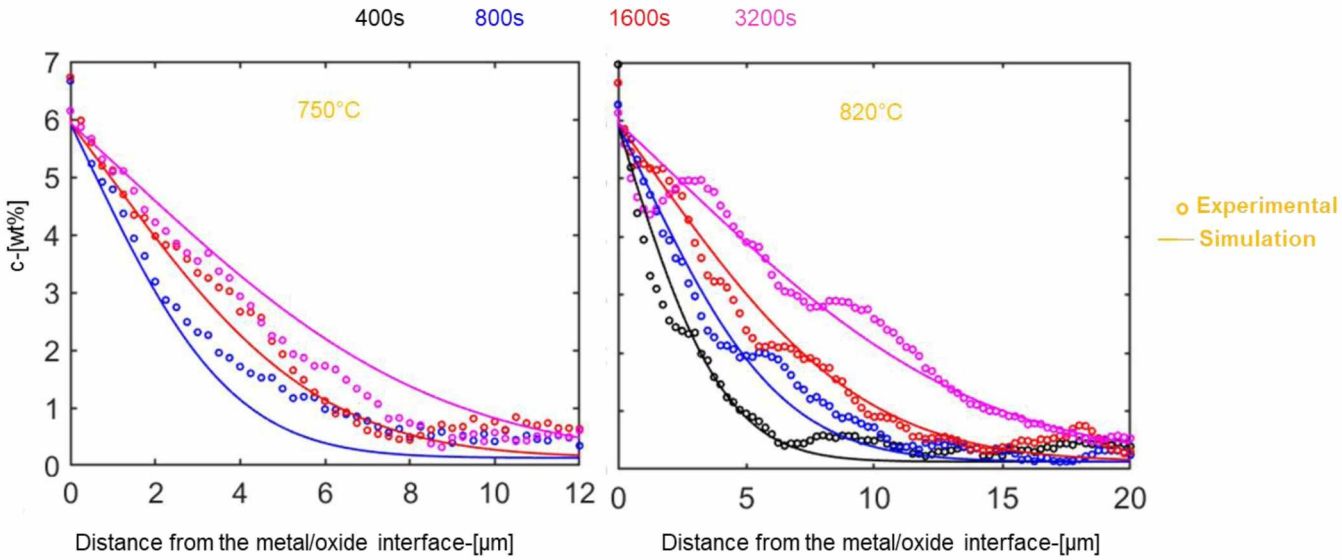

Fig 7: Oxygen profile in α(O) layer at 750°C and 820°C after several durations at high-temperature.

The metal diffusion coefficients identified in this work are consistent with those available in the literature:

	$D_m(cm^2/s)$	
	This work	(Ritchie,1997) [5]
750°C	5.78×10^{-11}	9.01×10^{-11}
820°C	1.49×10^{-10}	3.87×10^{-10}

Tab 4: Comparison of the identified metal diffusion coefficients with those in the literature.

Let us assume that c_s represents the threshold oxygen concentration at which the α(O) becomes visible on an optical metallography. The α(O) layer thickness can then be determined from the oxygen profiles by measuring the distance between the metal/oxide interface and the depth where the oxygen concentration is c_s (cf. Fig 8):

$$e^{c_s}_{\alpha^{\mu}(O)} = D_{c=c_s} - D_{c=c_{m/o}} \quad (5)$$

$D_{c=c_s}$: distance from the external surface to the depth where the oxygen concentration is $c = c_s$,

$D_{c=c_{m/o}}$: distance from the external surface to the depth where the oxygen concentration is $c = c_{m/o}$,

$c_{m/o}$: concentration at the metal/oxide interface on the metal side (Fig 7),

$e^{c_s}_{\alpha^{\mu}(O)}$: α(O) layer thickness determined using the oxygen profile.

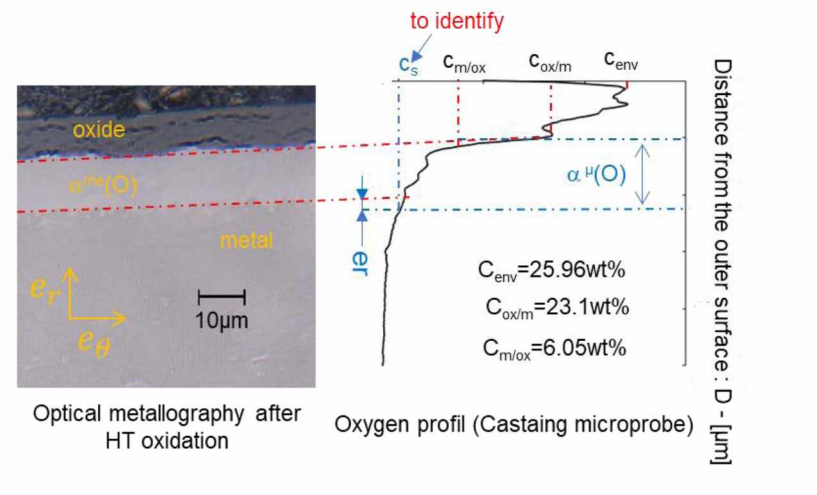

Fig 8: Comparison of the optical metallography with the corresponding oxygen profile.

The difference between metallography and microprobe is given by:

$$er(c_s) = e^{c_s}_{\alpha^{\mu}(O)} - e_{\alpha^{me}(O)} \tag{6}$$

The least squares minimization of this functional $er(c_s)$ run on all tests leads to a threshold concentration of This value represents the minimum concentration from which the α(O) layer becomes visible on an optical metallography for temperatures between 750°C and 820°C. This value is consistent with the concentration of oxygen in the α(O) layer for oxidation at higher temperatures (T>900°C).

3.2. Ballooning test results

Fig. 9 shows the strain profile of the ballox3 sample after 1000s of creep. The thermal profile at the same time is also shown. Under axisymmetric assumption, the strain calculated in the image plane is equivalent to the circumferential strain of the sample:

$$\varepsilon = \frac{\Delta l}{l_0} = \frac{U_r}{R_e} \tag{7}$$

l: ROI width (Fig 9)
U_r: radial displacement of the external surface,
R_e: external radius of the sample.

The thermal and kinematic profiles are consistent with creep in the alpha domain [2, 3], the strain is maximal at the hottest point.

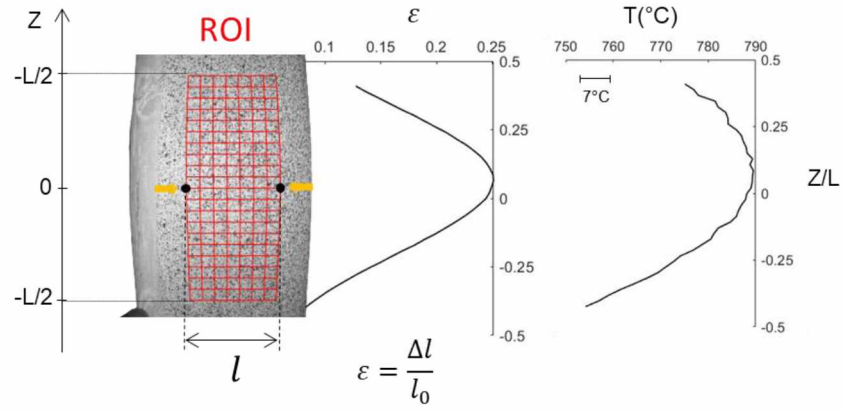

Fig 9: Strain and thermal profile after 1000s of creep at T=800°C and p=30bar.

Fig 10 shows the time evolution of the maximum strain (identified by the arrows in Fig 9) for the five tests performed. For all these tests, the temperature was stabilized around 800°C. The temperature difference between all the tests is lower than 10°C (see tab3) allowing direct comparision between the test results.

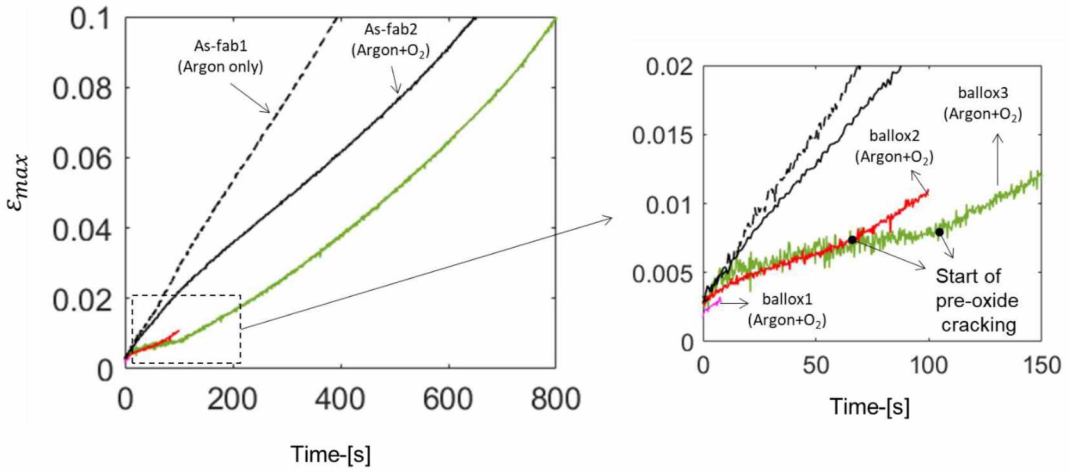

Fig 10: Strain versus time at the center of the ROI (where the strain is maximum) during ballooning test at T=800°C and p=30bar.

Creep increases linearly with time on the test performed under argon on an as-fabricated sample (As-fab1). For the test carried out in an atmosphere containing a mixture of argon and oxygen, the strain follows a linear trend at the beginning and then gradually the strain rate decreases due to a reinforcement effect of the oxide and α(O) layers which are formed during the test. The reinforcement effect of α(O) is a well-known effect in the literature [5]. For tests on pre-oxidized samples, the strain rate is low at the beginning of the test. After a certain time,a strain runaway is observed. Optical metallography (Fig. 11) was performed on the 3 pre-oxidized samples.

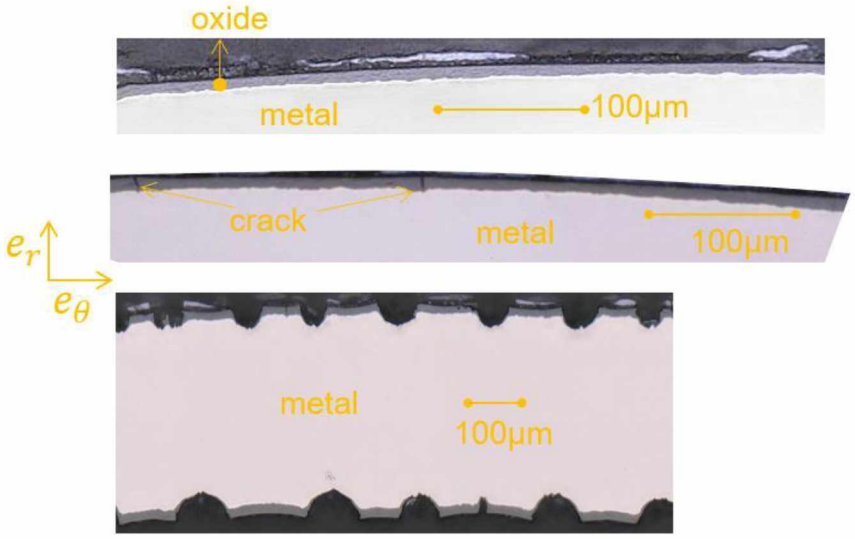

Fig 11: Optical metallography after ballooning tests under Argon+O_2, p=30bar and T=800°C, the tests on the ballox1 and ballox2 samples were interrupted respectively after 10 and 100s of creep, the one on ballox3 was carried out until the burst.

No oxide cracks are present in the test interrupted after 10s (ballox1). Few cracks are present for the test interrupted after 100s (ballox2) just after the strain runaway. For the test until burst (ballox3), a larger number of cracks is observed. This result highlights the fact that the strain runaway is due to the cracking of the oxide.

The oxide plays a reinforcing role at the beginning of the test as long as it is not cracked. Once cracked, the deformations are localized between the oxide fragments where the metal is exposed, leading to a runaway of the macroscopic strain. The cracking of the oxide occurs continuously during the ballooning. This continuous cracking process of the inner and outer oxide layers leads to a complex evolution of the macroscopic strain.

4. Conclusion

HT oxidation tests on as-fabricated and pre-oxidized Zircaloy-4 samples were performed at 750°C and 820°C. A cubic kinetics is observed for oxide growth at these temperatures. The growth kinetics of the oxygen enriched metal layer (α(O)) is consistent with the extrapolation of the correlation established by other work [1] on tests performed at higher temperatures (T>900°C) which was not obvious because the material undergoes a phase transformation between 820 and 900°C. An oxygen content of 1.27wt% represents the minimum concentration above which the α(O) layer can be revealed using optical metallography for temperature between 750°C and 820°C. The metal oxygen diffusion coefficient has also been identified at 750°C and 820°C.

Ballooning tests were performed at 800°C under internal pressure of 30 bar. These tests highlighted the reinforcing role played by the HT oxide, α(O) and pre-oxide layers against ballooning, as long as the pre-oxide is not cracked. Once cracked, the strain is localized between the fragments of oxide where the metal is exposed to the environment, which leads to a runaway of macroscopic strain. Cracks can continue to propagate at a rate controlled by the oxidation of the exposed metal. The cracking of the oxide occurs continuously during the ballooning process. This leads to a complex evolution of the macroscopic strain after the initiation of the cracking of the oxide.

In perspective, these ballooning tests will be simulated. The oxygen diffusion coefficients identified in the metal will allow to consider the effect of oxygen on creep.

References

[1] J. Desquines, C. Duriez, S. Guilbert, et T. Taurines, « High temperature oxidation and room temperature axial strength of pre-oxidized zircaloy-4 cladding after a simulated LOCA », *Journal of Nuclear Materials*, vol. 543, p. 152559, janv. 2021, doi: 10.1016/j.jnucmat.2020.152559.

[2] T. Jailin *et al.*, « Mechanical behavior of as-fabricated Zircaloy-4 claddings under the simulated thermo-mechanical post-DNB conditions of a Reactivity Initiated Accident (RIA) », p. 10.

[3] D. Campello, N. Tardif, M. Moula, M. C. Baietto, M. Coret, et J. Desquines, « Identification of the steady-state creep behavior of Zircaloy-4 claddings under simulated Loss-Of-Coolant Accident conditions based on a coupled experimental/numerical approach », *International Journal of Solids and Structures*, vol. 115-116, p. 190-199, juin 2017, doi: 10.1016/j.ijsolstr.2017.03.016.

[4] F. Nagase, T. Otomo, et H. Uetsuka, « Oxidation Kinetics of Low-Sn Zircaloy-4 at the Temperature Range from 773 to 1,573K », *Journal of Nuclear Science and Technology*, vol. 40, nº 4, p. 213-219, avr. 2003, doi: 10.1080/18811248.2003.9715351.

[5] I. G. Ritchie et A. Atrens, « The diffusion of oxygen in alpha-zirconium », *Journal of Nuclear Materials*, vol. 67, nº 3, p. 254-264, août 1977, doi: 10.1016/0022-3115(77)90097-6.

[6] R. Chosson, A. F. Gourgues-Lorenzon, V. Vandenberghe, J. C. Brachet, et J. Crépin, « Creep flow and fracture behavior of the oxygen-enriched alpha phase in zirconium alloys », *Scripta Materialia*, vol. 117, p. 20-23, mai 2016, doi: 10.1016/j.scriptamat.2016.02.021.